Robotica (2016) volume 34, pp. 2878–2891. © Cambridge University Press 2016
doi:10.1017/S0263574716000011

Effects of head and tail as swinging appendages on the dynamic walking performance of a quadruped robot

Xiuli Zhang*, Jiaqing Gong and Yanan Yao

School of Mechanical, Electronic and Control Engineering, Beijing Jiaotong University, Beijing 100044, China

(Accepted January 4, 2016. First published online: March 14, 2016)

SUMMARY
We designed a quadruped robot with a one-degree-of-freedom (1-DOF)-pitch head, a 1-DOF-roll tail, and 14 active DOFs in total, which are controlled via a central pattern generator (CPG) based on a Hopf oscillator. Head and tail movements are coupled to the leg movements with fixed phase differences. Experiments show that tail swinging in roll can equilibrate feet–ground reaction forces (GRF), reducing yaw errors and enabling the robot to maintain its direction when trotting. Head swing in pitch has the potential to increase flight time and stride length of the swinging legs and increase the robot's forward velocity when running in bounds.

KEYWORDS: Quadruped robot, Swinging appendage, Rhythmic motion, Biologically inspired, Central pattern generator

1. Introduction

Most legged animals have body segments consisting of legs/arms, trunk, head, and tail, which allows for rough classification. Scientists and engineers have long sought to understand why the bodies of legged animals are not constructed as a single rigid frame, and how different body segments facilitate animals' functional locomotion. Various hypotheses have been presented based on abundant observations of animals. The hypotheses provided engineers with solutions to problems in robot design and control. As for legged animals, legs are mainly used for locomotion; however, the role of other body segments, such as tails and heads, which we consider as appendages for locomotion, remains poorly understood. Also, there are few examples of effective head and tail use in robots.

Tail use in lizards, cheetahs, cats, and kangaroos has been broadly investigated. It has been agreed that an animal's tail works as an inertia appendage to stabilize or redirect its body during dynamic and irregular movements.[1] Lizards have been observed using their tails in aerial maneuvers for self-righting and air-turning.[2–4] Libby *et al*. revealed that lizards control the swinging of their tails in a measured manner to redirect angular momentum from their bodies to their tails, stabilizing body attitude in the sagittal plane.[5] Lizard-inspired robots have been built with active tails that function as effectively as those in their animal counterparts to adjust the body's pitch or roll movement.[6,7] The cheetah's ability to turn rapidly during a chase is enabled by swinging its long, powerful tail.[8] Small cats use their tails to balance on branches or walls.[9] Inspired by the above examples, Briggs *et al.* attached a 2-DOF tail to the biomimetic MIT Cheetah robot and modeled the robot as a two-link system with a joint. They proved theoretically that the body and tail appendage conserve angular momentum in mid-air, which means that the change in the absolute angle of the body is linearly related to the change in the angle of the tail appendage. Using tail control enabled the Cheetah robot to perform aerial orientation maneuvers in simulations, and to reject an impulsive disturbance from a wrecking ball in experiments.[10] Patel and Braae conducted similar studies on their quadruped robot, Dima.[11,12]

* Corresponding author. E-mail: zhangxl@bjtu.edu.cn

Kangaroos use their tails as a counter-balance during standing and for energy storage during hopping.[13] Zeglin,[14] Liu *et al.*[15] and the Festo Company built bionic kangaroos that were able to realistically emulate the animal's jumping behavior. The tail is used to compensate for the torque generated during the flight phase as the legs are pulled forward, thereby maintaining the top of the body horizontally. For humans, the two arms are inertial swing appendages that function as dynamic stabilizers during bipedal walking.[16,17] The Boston Dynamics group's humanoid Atlas maintains its balance against an impact force when standing on one leg by swinging its arms. Similarly, in Primer-V4, the bipedal tightrope walker built by Yamaguchi, the arms and upper body play a critical role in shifting the robot's center of gravity to keep it balanced.[18]

Salamanders have the ability to locomote in different environments using different motion patterns. Karakasiliotis and Schilling *et al.* has published a review on the kinematics of salamanders' locomotion for each body part of the salamander in terrestrial stepping and swimming. Their experiments using a salamander-like robot revealed the tail's role on influencing the robot's speed in terrestrial stepping as the robot's stride length was decreased when its tail was removed, and the stride length was increased when the tail was oscillating with higher bending values. They also mentioned Cabelguen's observations that salamanders use the tail as a "fifth limb" oscillating at high amplitudes to help it walking on slippery surfaces.[19–21] Many birds show obvious head-bobbing when they walk. Most work supported the viewpoint that the head plays an important role in stable vision acquisition in birds.[22–24] Heads were used in robots to develop stable vision too. Santos[25] developed a CPG-based head controller that was able to reduce the head motion induced by locomotion itself. Mederreg's RoboCoq was designed as an autonomous bipedal robot with stabilized vision based on the avian model.[26] However, an easily observed fact is horses and greyhound dogs swing their heads in pitch during high speed running and these head movements are commonly synchronized with leg movements. That suggests the head may have effects on facilitating locomotion other than stabilizing vision. Unfortunately, there are few studies on how heads interplay with legs to facilitate efficient locomotion in animals, and even fewer head use in legged robots are there.

In this study, we try to investigate how head and tail, working as swing appendages, facilitate locomotion using a quadruped robot Dcat. We described Dcat robot's physical structure and its gait controller (a CPG model without feedbacks) in Section 2. Dcat has originally no head and tail just like most quadruped robots in the world. We found that Dcat was not able to follow the correct direction when trotting. Also, when Dcat runs in bounds, it stumbles easily and does not run as fast as intended. In Section 3, we analyzed the robot's trotting behavior using a reasonably simplified mechanical model to seek the possible reasons for the deviation of the robot. In addition, we observed how a greyhound swings its head when bounding and present a hypothesis of the purpose of the head swing. Based on the theoretical analyses and the hypothesis, we present the approaches of implementing a biomimetic head and tail in Dcat to improve its locomotion and furthermore to elucidate how the head and tail can influence body movements. Then, we used physical experiments to verify the correctness of the theoretical analysis and the effectiveness of our control approaches (Section 4). Discussions about the inherent physical imbalance of a robot, head and tail DOF configuration, and CPG parameter determination are described in Section 5. We draw conclusions about how the head and tail influence walking performance in Section 6.

2. Quadruped Robot Dcat and CPG Controller

2.1. Dcat physical prototype

The quadruped robot Dcat is shown in Fig. 1. Each of the robot's legs has three joints: hip, knee, and ankle. The hip joints have 2-DOF, pitch and roll; the knee joints have one pitch DOF; and the ankles are spring damper passive joints with one prismatic DOF. The head and the tail consist of a carbon fiber rod with a dumbbell at the tip. The head has one pitch DOF and the tail has one roll DOF. The dumbbells are designed to be 5% of the weight of the robot. All 14 active joints are driven by Maxon DC motors. The robot is equipped with photo encoders on each joint, which are used for lower level PID control, an Mti inertia measurement unit (IMU from Xsens Technologies B.V.) on the trunk, and FSR force sensors (FlexiForce Group) on the bottom of each foot. The IMU and FSR sensors are used for evaluating the robot's performance only. The physical specifications of Dcat are listed in Table I.

https://doi.org/10.1017/S0263574716000011 Published online by Cambridge University Press

Table I. Dcat's physical specifications..

Item	Mass (kg)	Dimensions (mm)
Trunk	1.834	430 × 150
thigh	0.492	150
shank	0.169	150
head	0.25	200
tail	0.25	300
whole robot	5.562	430×150×350

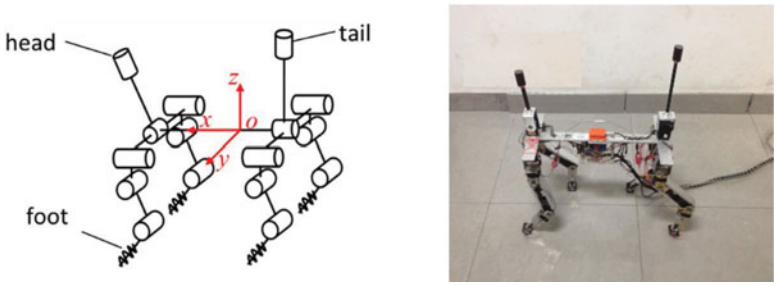

Fig. 1. The quadruped robot, Dcat.

2.2. *CPG controller*

It is believed that rhythmic activities in animals are controlled by CPGs—networks of neurons in vertebrate spinal cords and invertebrate thoracic ganglia—capable of generating rhythmic muscular activity in the absence of sensory feedback.[27] However, there is ongoing debate, which counters that CPGs do not lead to stable or directed walking, and sensory feedback plays an important role in regulating locomotion in animals.[28,29] Generally modeled as networks of coupled oscillators/neurons, the biologically inspired CPGs have advantages in coupling many DOFs to generate harmonious motion patterns. Being simple yet robust, CPGs are employed for locomotive control in various robots, such as swimming in a salamander-like robot[30] and a robotic fish,[31] and walking in a quadrupedal robot.[32] In this paper, we employed CPGs to construct a stable coupling between the head, tail and legs in Dcat. Using a Hopf oscillator, a CPG model was built to generate angular trajectories for Dcat.

2.2.1. Hopf oscillator. The Hopf oscillator is defined by the following equations.[33]

$$\begin{cases} \dot{u} = \alpha(\mu^2 - r^2)u - \omega v, \\ \dot{v} = \delta(\mu^2 - r^2)v + \omega u, \\ \\ r = \sqrt{u^2 + v^2}, \\ \omega = \frac{\omega_{\mathrm{st}}(e^{bv}+\eta)}{e^{bv}+1}, \\ \eta = \frac{\omega_{\mathrm{sw}}}{\omega_{\mathrm{st}}}. \end{cases} \tag{1}$$

where r, μ, and ω denote the limit cycle radius, amplitude, and angular frequency of the Hopf oscillator, respectively; ω_{st} and ω_{sw} are the respective angular frequencies of the stance phase and the swing phase of the robot walking cycle; u and v are the status variables and α and δ are their respective convergence efficiencies; and b is an integration constant. We use u and v as angular position control signals for the hip and knee joints, respectively.

2.2.2. The coupled CPG network. To control Dcat's 14 active DOFs to generate coordinated rhythmic movements, a CPG model is built by coupling 15 Hopf oscillators together to structure a network. The couplings form two layers among the oscillators: the inter-limb layer and the intra-limb layer, as shown in Fig. 2. The inter-limb layer is between the legs, the head, and tail, using Oscillator 0 as a reference. Oscillators 1–4 for the hip pitch DOFs, 13 for the head and 14 for the tail couple with Oscillator 0 through phase differences φ_i^0 (i = 1–4, 13, 14), thereby generating different gaits for the robot. The intra-limb layer is between the different joints in the same leg, using the leg's hip

https://doi.org/10.1017/S0263574716000011 Published online by Cambridge University Press

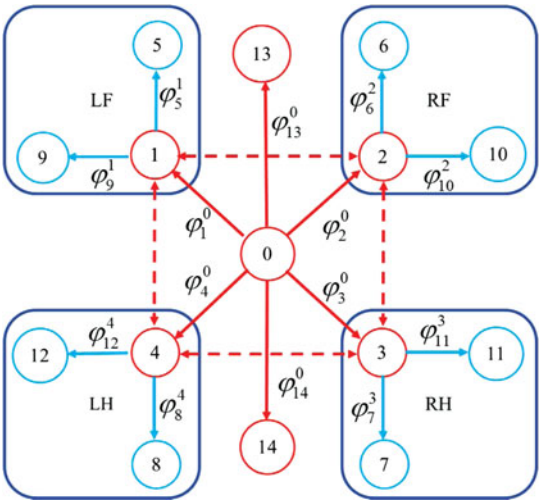

Fig. 2. Model of the central pattern generator. 1: LF hip pitch, 2: RF hip pitch, 3: RH hip pitch, 4: LH hip pitch, 5: LF knee, 6: RF knee, 7: RH knee, 8: LH knee, 9: LF hip roll, 10: RF hip roll, 11: RH hip roll, 12: LH hip roll, 13: head, 14: tail. LF, RF, LH and RH denote left-front, right-front, left-hind, and right-hind leg, respectively.

pitch oscillator as a reference. Oscillators 5–8 for the knee DOFs and Oscillators 9–12 for the hip roll DOFs couple with the hip pitch oscillator in their own legs through phase differences φ_i^{i-4} (i = 5–8) and φ_i^{i-8}(i = 9–12) to produce different foot trajectories.

The CPG controller is defined by the following equations.

$$\begin{cases} \left.\begin{aligned} \dot{u}_0 &= \alpha(\mu^2 - r^2)u_0 - \omega v_0 \\ \dot{v}_0 &= \delta(\mu^2 - r^2)v_0 + \omega u_0 \end{aligned}\right\} \quad (i{=}0) \\ \left.\begin{aligned} \dot{u}_i &= \alpha(\mu^2 - r^2)u_i - \omega v_i + k\left(u_{i-4}\cos\varphi_i^{i-j} - v_{i-4}\sin\varphi_i^{i-j}\right) \\ \dot{v}_i &= \delta(\mu^2 - r^2)v_i + \omega u_i + k\left(u_{i-4}\sin\varphi_i^{i-j} + v_{i-4}\cos\varphi_i^{i-j}\right) \end{aligned}\right\} \\ \quad (j = i \text{ if } i = 1{-}4, 13, 14;\ j = 4 \text{ if } i = 5{-}8;\ j = 8 \text{ if } i = 9{-}12) \\ \theta_i = A_i u_i + o_i \quad (i = 1{-}4, 9{-}14) \\ \theta_i = \left\{ \begin{array}{ll} 0 & (v_i < 0, \quad \text{stance}) \\ -A_i v_i + o_i & (v_i > 0, \quad \text{swing}) \end{array} \right\} (i = 5{-}8) \end{cases}, \tag{2}$$

where θ_i, A_i, and o_i are, respectively, the angular position, amplitude and reference position of the ith DOF, φ_i^{i-j} is the phase difference of Oscillator i relative to Oscillator i–j, and k is a coupling coefficient. The CPG parameters are determined mostly by trial and error for better performance, and the values are listed in the Appendix.

3. Effects of Swinging Appendages

3.1. Swinging tail

3.1.1. Observations. We found that the quadruped robot Dcat has some problems when it trots: (1) it drags its front feet; (2) there are large differences in the GRFs between the left and right feet; and (3) it is unable to maintain the intended bearing and always yaws to the right. It was observed that the robot has a tendency to topple to the side of the front swing leg, causing the foot of this leg to drag along the ground. As shown in Fig. 3, when legs LF and RH are in contact with the ground, the trunk rolls around the x axis in the positive direction (with respect to a right-hand coordinate system) and topples to the side of swing leg RF, causing foot RF to drag along the ground. When legs RF and LH are in contact with the ground, the trunk rolls around the x axis in the negative direction and topples to the side of leg LF, causing foot LF to drag along the ground. We believe that this contributes to the left and right feet having different GRFs and the robot yawing in a particular direction. To counteract

https://doi.org/10.1017/S0263574716000011 Published online by Cambridge University Press

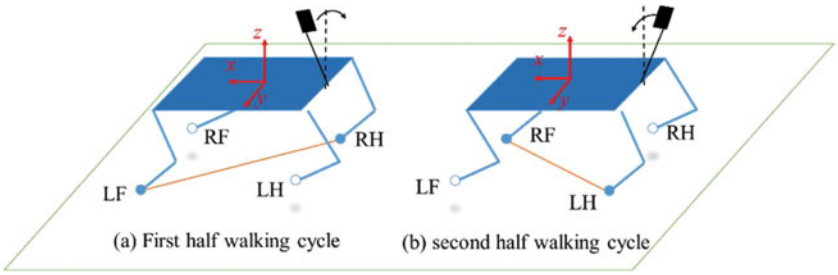

Fig. 3. Our implementation of tail swing locomotion. (Filled circles are the feet on the ground.)

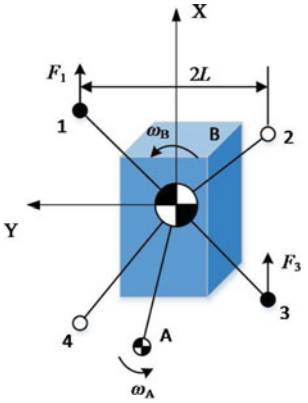

Fig. 4. Force and motion effects of the tail on the main body.

the toppling tendency of the trunk, we moved the tail with the following control protocol; that is, the tail moves in phase with leg LF. Therefore, when legs LF and RH are in contact with the ground, the tail rotates counterclockwise around the x axis (lean to right) to transfer a negative roll tendency to the trunk. When leg RF and LH are in contact with the ground, the tail rotates clockwise around the x axis (lean to left) to transfer a positive roll tendency to the trunk.

3.1.2. Mechanical analysis of swinging tail. The quadruped robot with an active tail is modeled as a two-body system, in which the tail is Body A and the trunk and four legs are Body B. A simplified force diagram in the XOY plane is shown in Fig. 4. The robot moves in a trot. Feet 1 and 3 are in contact with the ground to support the net body mass with forward friction forces F_1 and F_3, respectively. Feet 2 and 4 are swinging in the air. If there is a difference between F_1 and F_3, then a yaw moment M will be generated on body B. The robot will deviate to one side if there is a persistent moment difference between the first half and second half of the trot gait cycle. We now derive the mechanics behind this hypothesis.

In the first half of the trotting cycle, Feet 1 and 3 are in contact with the ground. The forward friction forces cause the moment M_{13} to act on body B,

$$M_{13} = F_3 L - F_1 L = I\dot{\omega}_{\mathrm{B}}. \tag{3}$$

We integrate Eq. (3) twice with respect to time over half the trotting cycle to compute the yaw angle of the robot,

$$\Omega_{13} = \frac{1}{I}\iint_{\frac{T}{2}} M_{13} d^2 t, \tag{4}$$

where T is the period of the trotting cycle. We repeat for the second half of the trotting cycle, in which Feet 2 and 4 are in contact with the ground. The forward friction forces cause the moment M_{24} and yaw angle Ω_{24} to act on body B,

$$M_{24} = F_2 L - F_4 L = I\dot{\omega}_{\mathrm{B}}, \tag{5}$$

https://doi.org/10.1017/S0263574716000011 Published online by Cambridge University Press

$$\Omega_{24} = \frac{1}{I}\iint_{\frac{T}{2}} M_{24} d^2t. \tag{6}$$

Let us suppose that there is a fixed moment difference, $\Delta M > 0$, between M_{13} and M_{24},

$$\begin{cases} M_{13} = M \\ M_{24} = M + \Delta M \end{cases} \tag{7}$$

We normalize by M to evaluate the degree of unbalance between the friction moments in the first half and the second half of the trotting cycle, which yields the average yaw angle of the robot,

$$\Delta\bar{\Omega}=\bar{\Omega}_{13}-\bar{\Omega}_{24}=\frac{1}{I}\iint_{\frac{T}{2}}\frac{M_{13}}{M}d^2t-\frac{1}{I}\iint_{\frac{T}{2}}\frac{M_{24}}{M}d^2t=\frac{1}{I}\iint_{\frac{T}{2}}\frac{-\Delta M}{M}d^2t=-\frac{\lambda\Delta M}{M}, \tag{8}$$

where $\lambda = \frac{T^2}{4I}$. The robot will turn towards the right when it has a negative yaw angle.

When the tail swings in the roll plane in-phase with the hip pitch DOF of the left front leg, the tail inertia moment causes an additional friction moment, Q, to act on body B,

$$Q = kI_{\mathrm{A}}\dot{\omega}_{\mathrm{A}}, \quad k > 0. \tag{9}$$

Therefore, the total friction moments acting on Body B during the first half and the second half of the trotting cycle are:

$$\begin{cases} M'_{13} = M+Q \\ M'_{24} = M + \Delta M + Q \end{cases}. \tag{10}$$

Normalizing by $M+Q$, the yaw angle of the robot becomes

$$\Delta\bar{\Omega}'=\frac{1}{I}\iint_{\frac{T}{2}}\frac{M'_{13}-M'_{24}}{M+Q}d^2t=\frac{1}{I}\iint_{\frac{T}{2}}\frac{-\Delta M}{M+Q}d^2t=-\frac{\lambda\Delta M}{M+Q}. \tag{11}$$

Therefore,

$$\left|\Delta\bar{\Omega}'\right| < \left|\Delta\bar{\Omega}\right|. \tag{12}$$

Thus the swing of the tail, synchronized with the legs but having an appropriate phase difference, can equilibrate the foot–GRFs to reduce the normalized unbalancing friction moments so as to decrease the yaw angle of the robot and allow the robot to retain its direction.

3.2. Swinging head

3.2.1. Observations. Six frames from the video of a greyhound running in bound gait published by Hudson[34] are shown in Fig. 5. They demonstrate how the greyhound's head swings rhythmically in pitch with a fixed phase relationship with the four limbs. During the first half of the running cycle, the two hind legs move backward during the stance phase and the two front legs swing forward in the swing phase, while the head swings downward, as shown in Fig. 5a–c. During the second half of the running cycle, the hind legs, the front legs and the head have movements opposite to those in the first half of the running cycle, as shown in Fig. 5d–f. Similar head movements are observed for other high speed running quadrupeds, such as horses.[35]

3.2.2. Dynamic analysis. For the situation (shown in Fig. 5a) in which the greyhound's hind legs are in stance and front legs are in swing, the force diagrams in the XOZ plane are shown in Fig. 6. Here, v_{B} and ω_{B} are the forward velocity and angular velocity, respectively, of the center of mass (COM) of the main body; v_{A} and ω_{A} are the forward velocity and angular velocity, respectively, of the head; and F is the force from the ground to the hind feet pointing to the COM of the main body.

https://doi.org/10.1017/S0263574716000011 Published online by Cambridge University Press

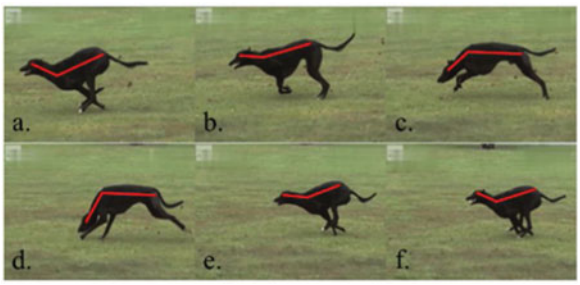

Fig. 5. Video frames of a greyhound running, demonstrating the head and torso positions.[31]

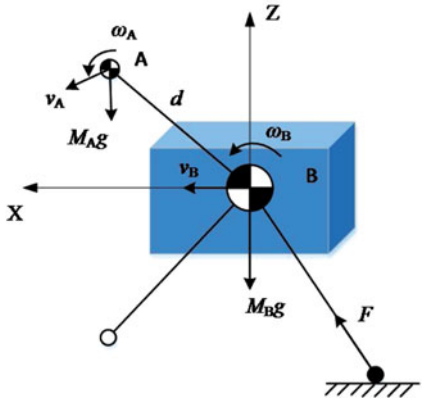

Fig. 6. Force and motion effects of the head on the main body.

The moments of the main body with respect to the system COM are

$$\vec{d} \times M_A g - \vec{d} \times M_A \dot{v}_A - I_A \dot{\omega}_A - I_B \dot{\omega}_B = 0, \tag{13}$$

where $\vec{d}$ is the vector from Body B to Body A, and

$$\dot{v}_A = \dot{v}_B + (\dot{\omega}_A + \dot{\omega}_B) \times \vec{d}. \tag{14}$$

Substituting Eq. (14) into (13) yields

$$\vec{d} \times M_A g - \vec{d} \times M_A(\dot{v}_B + \dot{\omega}_A d + \dot{\omega}_B d) - I_A \dot{\omega}_A - I_B \dot{\omega}_B = 0. \tag{15}$$

We define $|\vec{d}|=d$ and evaluate Eq. (15) in the XOZ plane, giving

$$I_A \left(1+\cos\frac{\Omega}{2}\right)\dot{\omega}_A + \left(I_B + I_A \cos\frac{\Omega}{2}\right)\dot{\omega}_B = M_A d \left(g \sin\Omega - \dot{v}_B \cos\frac{\Omega}{2}\right), \tag{16}$$

where $\Omega = \Omega_0 + \int\int \dot{\omega}_A d^2 t$, $\quad I_A = M_A d^2$, Ω is the angular position of Body A and Ω_0 is the angular reference position.

As the swing amplitude of the head is relatively small compared with its reference position, Ω can be approximated as a constant. We also consider the average translating velocity of the COM of body B to be constant; i.e., $\dot{v}_B = 0$. Therefore, Eq. (16) reduces to

$$I'_A \dot{\omega}_A + I'_B \dot{\omega}_B = H, \tag{17}$$

where H is the constant of integration, and I'_A and I'_B are the equivalent moments of inertia of Body A and Body B, respectively, which we approximate as constants. Integrating Eq. (17) twice with respect

https://doi.org/10.1017/S0263574716000011 Published online by Cambridge University Press

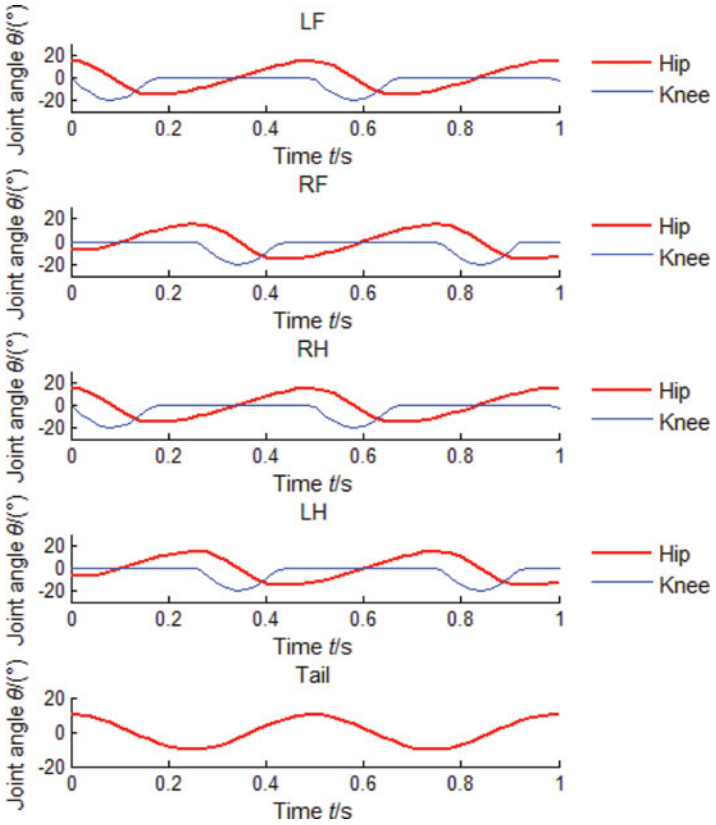

Fig. 7. Angular displacements of the hip and knee in the four legs and of the tail.

to time yields:

$$I'_{\mathrm{A}} \cdot \Delta\Omega_{\mathrm{A}} + I'_{\mathrm{B}} \cdot \Delta\Omega_{\mathrm{B}} = H^{*}. \tag{18}$$

Equations (17) and (18) describe the two-body system of the quadruped robot with an active head, which approximates—in the pitch plane—the law of conservation of angular momentum. In this two-body system, the change in the absolute angle of body A (head) can cause the opposite change in the absolute angle of body B. During the hind legs' stance phase, the head rotating downward (counterclockwise) can cause the main body to rotate upward (clockwise) with respect to the hind stance feet, giving the swinging front legs a longer flight time and a longer stride length. Similarly, during the front legs' stance phase, the head rotating upward (clockwise) can also cause the main body to rotate upward (counterclockwise) with respect to the front stance feet, thus the swinging hind legs gain a longer flight time and longer stride. As a result, the greyhound achieves greater speed.

4. Experiments and Results

4.1. Swinging tail experiments

The tail of the quadruped robot Dcat has a roll DOF that is controlled by Oscillator 14 of the CPG. We set the phase difference of tail oscillator with respect to Oscillator 0 to be zero, i.e., $\varphi_{14}^{0}=0$, according to the tail control protocol presented in Section 3.1, thereby the tail is directly coupled with Oscillator 0 and with the legs. The amplitude of Oscillator 14 was set to be $\mathrm{A}_{14}= 10^{\circ}$ by trial and error for good performance. The CPG outputs the angular displacements of the tail, hip, and knee DOFs, as shown in Fig. 7. We observed that the tail was swinging rhythmically and was synchronized with the four legs, moving in-phase with legs LF and RH in a trot gait.

We conducted experiments in which Dcat trotted with either an active or fixed tail. The active tail locomotion snapshots are shown in Fig. 8 and the GRFs for each foot are shown in Fig. 9. From the

https://doi.org/10.1017/S0263574716000011 Published online by Cambridge University Press

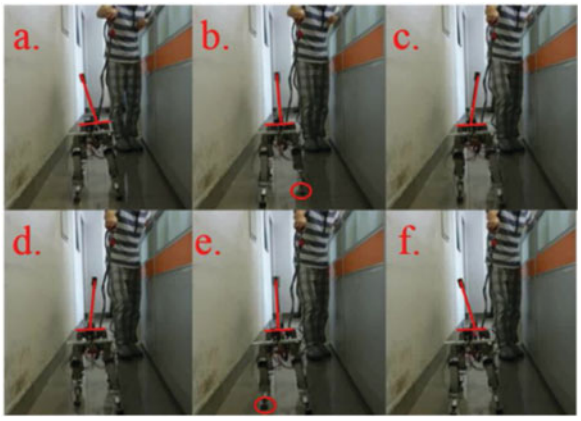

Fig. 8. Dcat robot ambulating in trot with an active tail.

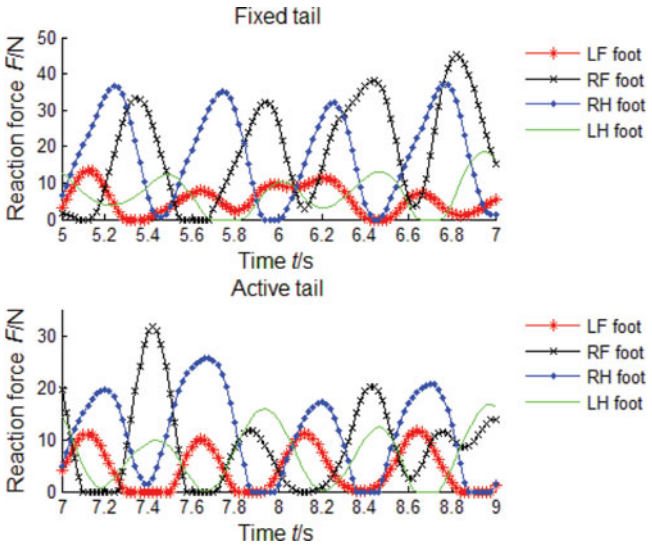

Fig. 9. Ground reaction forces for each foot in trot motion.

latter, we see that there are relatively small differences in the GRFs between the left and right feet when the robot walks with an active tail. In contrast, when the tail is fixed, the left-to-right variation of the GRFs increases. Figure 10 plots the trunk's angular displacement in yaw. We observe that for the same period of locomotion (8 gait cycles), the fixed-tail robot deviates to the right with almost 20° yaw error, while the active-tail robot experiences swings of ± 2.5° in yaw and holds its straight path. The active-tail robot is able to reach a forward velocity of 0.402 m/s. These experimental results demonstrate that a tail, working as a swing appendage for a robot ambulating with a trot gait, can strengthen the locomotion rhythm of the whole system. This improvement effectively equilibrates the GRFs of all feet and decreases yaw error to ensure that the robot moves in the intended direction.

4.2. Swinging head experiments

Here, we present the head control protocol of the Dcat running in a bound gait according to greyhound running motion (Fig. 6) with the assumption of achieving higher speed as analyzed in Section 3.2. We specify that the head moves in-phase with the hind legs, setting the parameters of head Oscillator 13 in the CPG to be $A_{13}= 15^{\circ}$, $\beta_{13}= 0.5$ and $\varphi_{13}^{0}=\pi$. The CPG outputs the angular displacements of the head, hips, and knees, as shown in Fig. 11.

We conducted experiments for the Dcat running with either an active or fixed head. The active-head snapshots are shown in Fig. 12 and the two GRFs from the left feet are shown in Fig. 13. We observed that the GRFs of the front and hind feet became of comparable magnitude with the introduction of the active head motion. The GRFs also varied more smoothly for the robot with an active head. The

https://doi.org/10.1017/S0263574716000011 Published online by Cambridge University Press

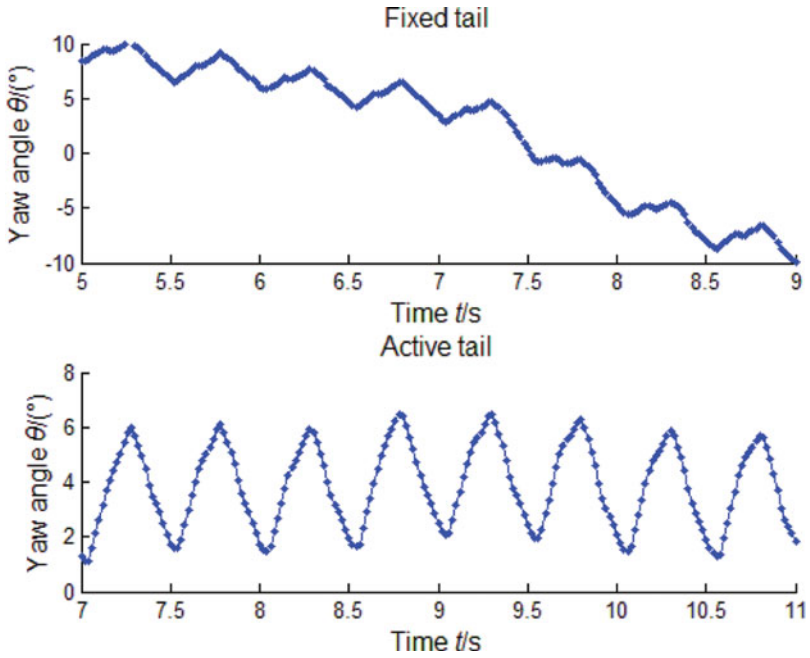

Fig. 10. Yaw angles of the trunk with fixed tail (above) and active tail (below).

trunk pitch angles are shown in Fig. 14. The robot with an active head has less variation in amplitude of the pitch angle oscillations owing to the anti-gravity trunk rotation caused by head swinging. The GRFs and trunk pitch angles demonstrate that posture stability is improved in the robot and there is a steadier rhythm reached throughout the gait cycle. We performed a series of 10 bounding experiments to measure the robot's running velocity. The average velocity was 0.604 m/s for the robot with the active head and 0.458 m/s for the robot with the head fixed, equaling a difference of 31.9%. These results agree with the predictions made from analyzing greyhound running.

5. Discussion

A legged robot with multi-DOFs is a complex system, in which locomotion happens as a stable rhythmic activity owing to the global interactions among the physical robot, CPG control and the environment. Mechanical imbalance, such as COM offset, is inherent in a physical robot because an asymmetrical mechanical structure is unavoidable in practical applications. Trajectory error is another inherent factor existing in a robot. The mechanical imbalance and trajectory error will cause unstable movement in the robot, such as yaw error in the trotting Dcat and the left–right GRFs differences for the bounding Dcat. There are many solutions to help a legged robot walking better. Trying to create a physically balanced robot is probably feasible but very difficult because the robot changes its shape and mechanical configuration when it walks dynamically. Balance control involve carefully and timely manipulating multiple joints of all legs. We assumed head and tail play important role in facilitating locomotion based on animal observations. Inspired by this, we try to solve deviation and unbalanced GRFs in Dcat robot through the control of head and tail. By coupling the head and tail with the legs the unstable walking of the robot Dcat has been improved obviously.

The DOF configuration of head and tail is usually task-oriented in a robot. From the viewpoint of mechanics, there are no major differences between using the head or tail as the inertial appendage except the bearing of different swinging directions (i.e., DOF configuration). There are normally three DOFs in an animal's head and tail, but we restricted them to a single DOF that plays the main role in a specific aspect of locomotion. For the head, the DOF in pitch is may help to increase forward speed for a quadruped robot. For the tail, the change in movement direction in yaw for a quadruped robot is assumed to benefit from a yaw or roll DOF. We chose a roll tail for Dcat, because a roll tail looks more natural and makes a more compact body for the robot than a yaw tail.

https://doi.org/10.1017/S0263574716000011 Published online by Cambridge University Press

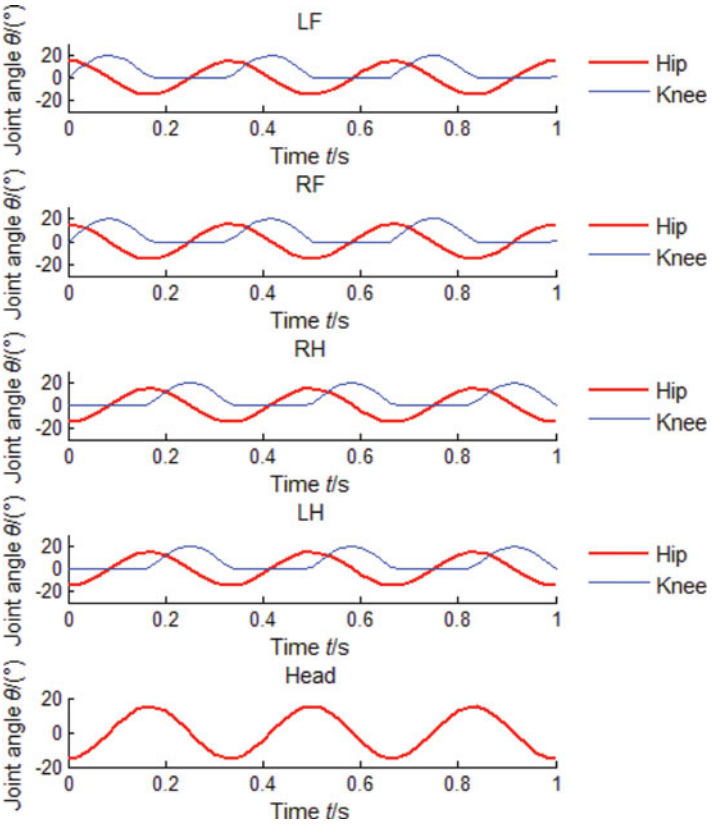

Fig. 11. Angular displacements of the hip and knee in the four legs and of the head.

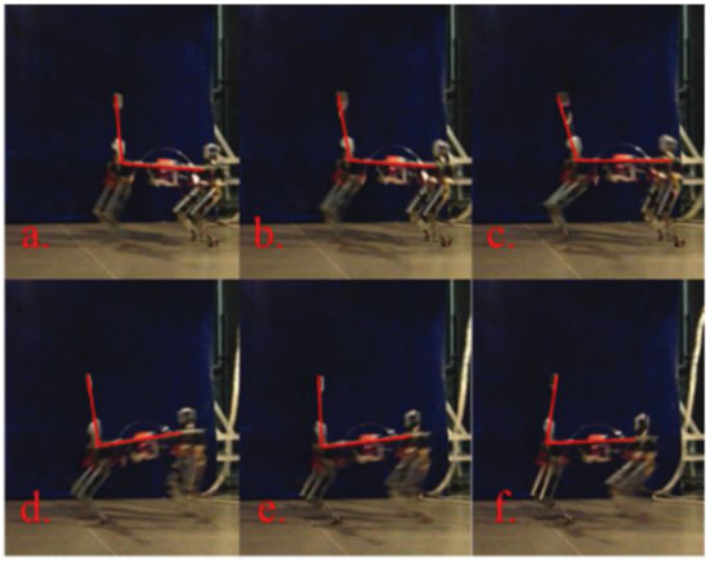

Fig. 12. Dcat robot running in bounds with an active head.

We investigated a pitching head for bounding gait and a rolling tail for trotting gait in the Dcat. The reasons why we did not couple the head and tail together or investigate head and tail use for different gaits are as follows. In our opinion, head and tail uses in animals are task-oriented. They may not use their heads and tails equally for a scenario; instead, they use one or the other as the major means to maneuver their movements in a certain situation, such as using the head to improve forward speed and the tail to change direction. Moreover, we think that animals use their heads or

https://doi.org/10.1017/S0263574716000011 Published online by Cambridge University Press

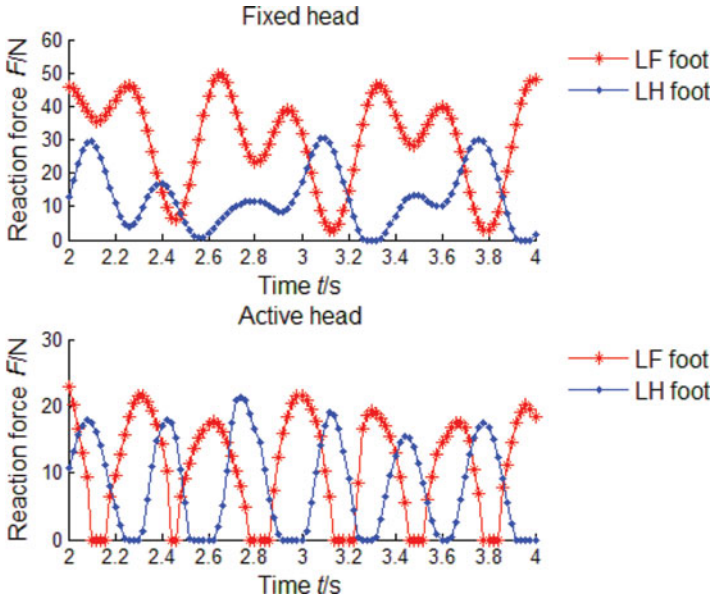

Fig. 13. Ground reaction forces of the left limbs for bound running.

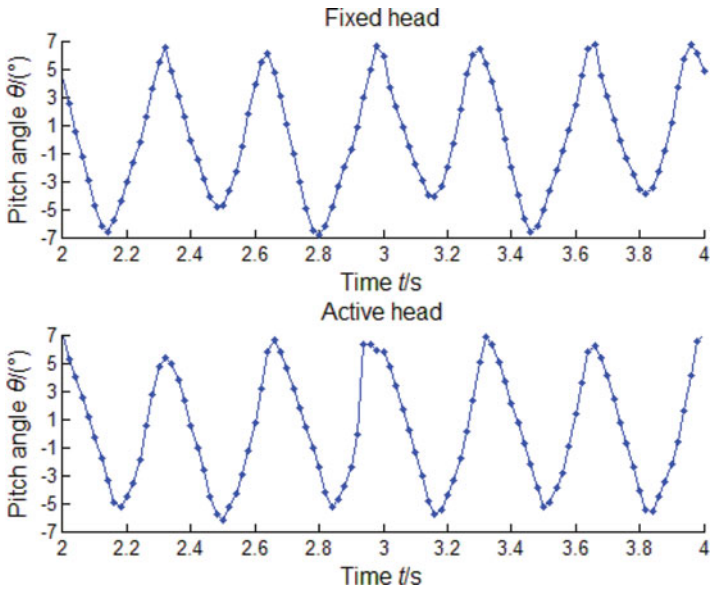

Fig. 14. Pitch angles of the trunk during bound running for the Dcat robot with a fixed head (above) and with an active head (below).

tails differently for different motion patterns or gaits. For example, some birds bob their heads when they walk, but not when they fly. Similarly, quadruped animals do not use their heads and tails for all gaits. We investigated head use in bounding and tail use in trotting separately because these two situations are highly useful for understanding the head and tail's effects on locomotion.

We used Hopf oscillator based CPGs to control all active DOFs in the Dcat, including coupling the head and tail with the legs. These biologically inspired CPGs have advantages in coordinating many DOFs to form stable rhythmic activity because of their limit cycle dynamics. The head or tail is synchronized with the legs, and the whole system status reaches a stable limit cycle. On this premise, the head and tail can maneuver the robot's movement. However, locomotion is a collective act involving between the robot mechanical dynamics, the CPG controller, and the environment. Tuning CPG parameters is quite a difficult job owing to the global entrainment of locomotion in the whole system. Some parameters in the Hopf oscillator have clear physical meaning when applied to

https://doi.org/10.1017/S0263574716000011 Published online by Cambridge University Press

robot control, such as the amplitude for a rotating joint. However, most parameters need to be tuned by trial and error, because there are strong coupling relationships between the parameters. In this paper, the head and tail oscillators' amplitudes were set by trial and error for a satisfactory performance for a certain gait.

6. Conclusions

We investigated how the head and tail, working as swing appendages, influence the main body movements of legged robots. We constructed a quadruped robot, Dcat, with a 1-roll-DOF tail and a 1-pitch-DOF head, and developed a CPG model based on a Hopf oscillator to control its 14 active joints and coordinate the phase relations among these joints. The biomimetic controllers for the head and tail oscillators were designed from observations of greyhound running and dynamic analysis. We performed experiments on Dcat. The results show that the swinging head and tail function as inertial appendages, equilibrating the GRF of the feet and enhancing the rhythm of the whole gait cycle. The tail swinging in roll decreases yaw errors and maintains the robot's intended direction when trotting, and the head swinging in pitch extends the swinging legs' flight time and stride length and increases the robot's forward velocity when running in bounds. Studying the biomechanical roles of the head and tail using a robot can advance our understanding of appendage evolution and provide biological inspiration for the next generation of maneuverable search-and-rescue robots.

Acknowledgements

This work was supported by the Fundamental Research Funds for the Central Universities of China with Grant M15JB00250.

References

1. G. Hickman, "The mammalian tail: A review of functions," *Mamm. Rev.* **9**(4), 143–157 (1979).
2. A. Jusufi, D. I. Goldman, S. Revzen and R. J. Full, "Active tails enhance arboreal acrobatics in geckos," *Proc. Natl Acad. Sci. USA* **105**, 4215–4219 (2008).
3. A. Jusufi, D.T. Kawano, T. Libby, R.J. Full, "Righting and turning in mid-air using appendage inertia: reptile tails, analytical models and bio-inspired robots" *Bioinspir. Biomim.* **5**, 045001 (2010).
4. A. Jusufi, Y. Zeng, R. J. Full and R. Dudley, "Aerial righting reflexes in flightless animals," *Integr. Comp. Biol.* **51**, 937–943 (2011).
5. T. Libby, T. Moore, E. Chang-Siu, D. Li, D. Cohen, A. Jusufi and R. Full, "Tail-assisted pitch control in lizards, robots and dinosaurs," *Nature* **481**(7380), 181–184 (2012).
6. E. Chang-Siu, T. Libby, M. Tomizuka *et al*., "A Lizard-Inspired Active Tail Enables Rapid Maneuvers and Dynamic Stabilization in a Terrestrial Robot," *Proceedings of the International Conference on Intelligent Robots and Systems*, San Francisco, CA, USA (Sep. 25–30, 2011) pp. 1887–1894.
7. A. M. Johnson, T. Libby, E. Chang-Siu *et al*. "Tail Assisted Dynamic Self-Righting," *Proceedings of the Fifteenth International Conference on Climbing and Walking Robots*, Sage Publications Ltd, London, England (2012) pp. 611–620.
8. D. Attenborough, "The life of mammals: the complete series," BBC Episode 5: meat eaters (2002–2003).
9. C. Walker, "Balance in the cat: Role of the tail and effects of sacrocaudal transection," *Behav. Brain Res.* **91**, 41–47 (1998).
10. R. Briggs, J. Lee and M. Haberland, "Tails in biomimetic design: Analysis, simulation, and experiment," *Proceedings of the Intelligent Robots and Systems, 2012 IEEE/RSJ International Conference on*, Vilamoura-Algarve, Portugal (2012) pp. 1473–1480.
11. A. Patel and M. Braae, "Rapid turning at high-speed: Inspirations from the cheetah's tail," *Proceedings of the Intelligent Robots and Systems, 2013 IEEE/RSJ International Conference on*, Tokyo, Japan (2013) pp. 5506–5511.
12. A. Patel and M. Braae, "Rapid acceleration and braking: Inspirations from the cheetah's tail," *Proceedings of the Robotics and Automation, 2014 IEEE International Conference on*, Hong Kong, China (2014) pp. 793–799.
13. U. Proske, "Energy conservation by elastic storage in kangaroos," Endeavour **4**(4), 148–153 (1980).
14. G. J. Zeglin, *Uniroo-a One Legged Dynamic Hopping Robot* (Massachusetts Institute of Technology, USA, 1991).
15. G. H. Liu, H. Y. Lin *et al*., "Design of a kangaroo robot with dynamic jogging locomotion," *Proceedings of the System Integration, 2013 IEEE/SICE International Symposium*, Kobe, Japan (2013) pp. 306–311.
16. M. Pijnappels, "Armed against falls: The contribution of arm movements to balance recovery after tripping," *Exp. Brain Res.* **201**, 689–699 (2010).
17. P. E. Roos, "The role of arm movement in early trip recovery in younger and older adults," *Gait Posture* **27**, 352–356 (2008).

18. Dr. Guero's Amazing Tightrope Walking Robot (Video). http://www.robots-dreams.com/2012/10/dr-gueros-amazing-tightrope-walking-robot-video.html. Oct.19, 2012.
19. K. Karakasiliotis, N. Schilling,·J.-M. Cabelguen *et al.*, "Where are we in understanding salamander locomotion: Biological and robotic perspectives on kinematics," *Biol. Cybern.* **107**, 529–544 (2013).
20. M. Schilling, T. Hoinville, J. Schmitz *et al*., "Walknet, a bio-inspired controller for hexapod walking," *Biol. Cybern.* **107**(4), 397–419 (2013).
21. M. Schilling, J. Paskarbeit, T. Hoinville *et al*., "A hexapod walker using a hierarchical architecture for action selection," *Front. Comput. Neurosc.* **7-126**, 1–17 (2013).
22. R. Necker, "Head-bobbing of walking birds," *J. Comp. Physiol. A* **193**, 1177–1183 (2007).
23. M. Fujita, "Head-bobbing and non-bobbing walking of black-headed gulls (Larus ridibundus)," *J. Comp. Physiol. A* **192**(5), 481–488 (2006).
24. J. A. Nyakatura and E. Andrada, "On vision in birds: Coordination of head-bobbing and gait stabilises vertical head position in quail," *Front. Zool.* **11**(27) (2014).
25. C. Santos, M. Oliveira, A. Rocha *et al*., "Head Motion Stabilization During Quadruped Robot Locomotion: Combining Dynamical Systems and a Genetic Algorithm," *Proceedings of the Robotics and Automation, IEEE International Conference on*, Kobe, Japan (2009) pp. 2294–2299.
26. L. Mederreg, V. Hugel and P. Bonnin, "The RoboCoq Project - Modelling and Design of Bird-Like Robot Equipped with Stabilized Vision," **In**: *Climbing and Walking Robots: and Their Supporting Technologies* (G. Muscato and D. Longo, eds.) *6th International Conference on Climbing and Walking Robots*, Professional Engineering, Bury St Edmunds, UK (2003) pp. 761–768.
27. A. J. Ijspeert, "Central pattern generators for locomotion control in animals and robots: A review," *Neural. Netw.* **21**, 642–653 (2008).
28. K. Pearson, O. Ekeberg and A. Bueschges, "Assessing sensory function in locomotor systems using neuro-mechanical simulations," *Trends. Neurosci.* **29**(11), 625–631 (2006).
29. H. Cruse, V. Duerr and J. Schmitz, "Insect walking is based on a decentralized architecture revealing a simple and robust controller," *Philos. T. R. Soc. A*, **365**(1850), 221–250 (2007).
30. A. J. Ijspeert, A. Crespi, D. Ryczko *et al*., "From swimming to walking with a salamander robot driven by a spinal cord model," *Science* **315**(5817), 1416–1420 (2007).
31. T. Wang, Y. Hu and J. Liang, "Learning to swim: A dynamical systems approach to mimicking fish swimming with CPG," *Robotica* **31**, 361–369 (2013).
32. H. Kimura, Y. Fukuoka and A. H. Cohen, "Adaptive dynamic walking of a quadruped robot on natural ground based on biological concepts," *Int. J. Rob. Res.* **26**(5), 475–490 (2007).
33. V. Matos, C. P. Santos and C. M. A. Pinto, "A Brainstem-Like Modulation Approach for Gait Transition in a Quadruped Robot," *Intelligent Robots and Systems, IEEE/RSJ International Conference on*, St Louis, Missouri, USA (2009) pp. 2665–2670.
34. P. E. Hudson. Cheetah vs Greyhound - World's Fastest Dog in Super Slow Motion. BBC, Earth Unplugged-Slo Mo #29. https://www.youtube.com/watch?v=jc8Hno4M0Qs. Aug. 22, 2013.
35. C. Walton. Preakness 2014 Horse Race VIDEO - California Chrome - HD. https://www.youtube.com/watch?v=xLGZbeC1kzc. May 17, 2014.

Appendix:

Table A1. Parameter values of the central pattern generator.

Parameter	Value	Parameter	Value
μ	1	$[A_1, A_2, A_3, A_4]$	$[15^\circ, 15^\circ, 15^\circ, 15^\circ]$
α	5	$[A_5, A_6, A_7, A_8]$	$[20^\circ, 20^\circ, 20^\circ, 20^\circ]$
δ	50	$[A_9, A_{10}, A_{11}, A_{12}]$	$[0^\circ, 0^\circ, 0^\circ, 0^\circ]$
b	100	A_{13}	15°
k	0.5	A_{14}	10°
ω	$4\pi, 6\pi$	$[o_1, o_2, o_3, o_4]$	$[\pm 30^\circ, \pm 30^\circ, \pm 30^\circ, \pm 30^\circ]$
β_{1-14}	$\beta_{1-14} \in (0, 1)$	$[o_5, o_6, o_7, o_8]$	$[\pm 60^\circ, \pm 60^\circ, \pm 60^\circ, \pm 60^\circ]$
$[\varphi_1^0, \varphi_2^0, \varphi_3^0, \varphi_4^0, \varphi_{13}^0, \varphi_{14}^0]$	$\varphi_1^0 \in (0, 2\pi)$	$[o_9, o_{10}, o_{11}, o_{12}]$	$[0^\circ, 0^\circ, 0^\circ, 0^\circ]$
$[\varphi_5^1, \varphi_6^2, \varphi_7^3, \varphi_8^4]$	[0, 0, 0,0]	o_{13}	0°
$[\varphi_9^1, \varphi_{10}^2, \varphi_{11}^3, \varphi_{12}^4]$	[0, 0, 0,0]	o_{14}	0°

https://doi.org/10.1017/S0263574716000011 Published online by Cambridge University Press